DNA Nanostructures

DOI: 10.1002/anie.201204245

Fabrication of ssDNA/Oligo(ethylene glycol) Monolayers and Complex Nanostructures by an Irradiation-Promoted Exchange Reaction**

*M. Nuruzzaman Khan, Vinalia Tjong, Ashutosh Chilkoti, and Michael Zharnikov**

The macromolecular structure of DNA, its ability to hybridize, the diversity of non-natural nucleotides with unique functional groups that are available to perform chemistry on it, and enzymes that are capable of manipulating its sequence, structure, and topology provide rich opportunities for its use in clinical diagnostics, biosensors, gene therapy, and drug delivery.[1–3] Some of these applications rely on the immobilization of single-stranded DNA (ssDNA) onto a solid support, which is subsequently used for binding and detection of its complementary ssDNA target or for the recognition of DNA binding proteins.[4–6] A commonly used method for immobilization of ssDNAs is to functionalize them with a terminal reactive group that is selective for the surface of interest.[4,5] Depending on the particular application, immobilization can be performed either homogeneously over the entire surface or lithographically, resulting in an array of ssDNA spots.[4,7–9]

The hybridization activity of supported ssDNA depends on the packing density and molecular organization, which can be manipulated by diluting ssDNA with other molecules that have the same reactive group.[4,10–13] For a gold substrate, the diluent molecules of choice are short-chain alkanethiols (ATs)[4,12–16] or thiolated oligo(ethylene glycol)s (OEG-ATs).[8–11,17–21] OEG-ATs are especially attractive for applications in which the DNA comes into contact with complex biological fluids because of their ability to resist the adsorption of proteins. Strategies to prepare such mixed films include co-deposition,[8,11,17–19,21] backfilling,[9,19] and post-deposition by substitution.[20] In an alternative approach, ssDNA can be covalently conjugated to a terminal reactive functional group presented by the monolayer.[6,22,23] OEG-ATs are also frequently used to provide a protein-repelling background to ssDNA patterns. These patterns are usually prepared by one of the standard techniques such as microcontact printing, UV lithography, or drop casting by a syringe or microarrayer.[7–9] The preparation of the OEG-ATs background typically occurs by backfilling after deposition of the ssDNA on the surface.

Herein, we present a new and potentially universal approach to prepare both mixed ssDNA/OEG-AT films in a broad range of compositions and ssDNA/OEG-AT patterns of arbitrary form. We demonstrate the strength of the approach by combining it with surface-initiated enzymatic polymerization (SIEP) and sculpting complex DNA nanostructures. This approach is based on an irradiation-promoted exchange reaction (IPER) and electron-beam lithography (EBL). Generally, IPER gives control over the extent and rate of the molecular exchange between the primary monolayer and a potential substituent by electron irradiation of the monolayer with a suitable dose.[24] It works well with a monolayer comprised of methyl-terminated, short-chain ATs,[24,25] but is difficult to apply to OEG-ATs films, because of the inefficiency of promoted exchange (the molecules are too long) and contrast deterioration owing to non-promoted exchange occurring frequently in these systems.[26,27]

However, IPER works well with thiolated ssDNA as the substituent. The procedure is illustrated in Figure 1a. A primary monolayer of a test OEG-AT compound, HO-$(CH_2CH_2O)_3(CH_2)_{11}$SH (termed EG3; see Refs. [28] and [29] for its protein-resistance) was homogeneously irradiated with electrons or using EBL, resulting in preferential damage of the OEG chain parts and cleavage of thiolate–gold bonds.[27,29] Next, the film was incubated with a solution of a model thiolated homo-oligonucleotide, 5′-SH-$(CH_2)_6$-$d(A)_{25}$-3′ (termed A25SH) for the exchange reaction promoted by the irradiation defects. We used EBL to visually demonstrate the efficiency of IPER in substituting A25SH in an EG3 matrix. AFM clearly shows the formation of a nanoscale A25SH pattern against a background of the EG3 that spells "DNA" (Figure 1c and Supporting Information, Figure S1).

The proportion of the A25SH component in the mixed A25SH/EG3 monolayer can be precisely controlled by selection of the irradiation dose. As shown in Figure 2a, N1s photoemission (PE) spectra of the one-component A25SH monolayer and mixed A25SH/EG3 films prepared by IPER exhibit the characteristic two-peak signature of adenine at 399.3 and 401.1 eV[5,30] and the intensity of this signal increases with increasing irradiation dose, demonstrat-

[*] M. N. Khan, Prof. Dr. M. Zharnikov
Angewandte Physikalische Chemie, Universität Heidelberg
Im Neuenheimer Feld 253, Heidelberg (Germany)
E-mail: Michael.Zharnikov@urz.uni-heidelberg.de
Homepage: http://www.pci.uni-heidelberg.de/apc/zharnikov/
V. Tjong, Prof. A. Chilkoti
Department of Biomedical Engineering, Duke University
Box 90300, Durham, NC 27708-0300 (USA)

[**] This work has been financially supported by grants from DFG (ZH 63/9-3 and EC 152/4-1), DAAD scholarship to M.N.K., NSF grant CBET-1033621 to A.C., and by a Duke University Nanoscience Graduate Fellowship to V.T. A.C. also acknowledges support of the NSF through the Research Triangle MRSEC (NSF DMR-11-21107). We thank M. Grunze for support of this work and the Max-lab and BESSY II staff for their assistance.

Supporting information for this article is available on the WWW under http://dx.doi.org/10.1002/anie.201204245.

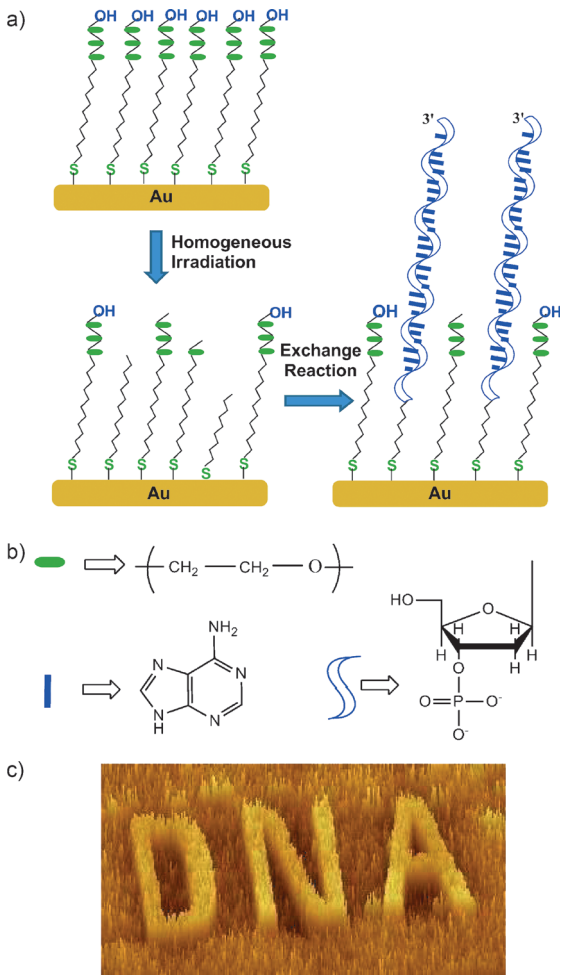

Figure 1. a) Schematic illustration of the approach. Irradiation-induced defects in the primary OEG-AT matrix promote an exchange reaction with the ssDNA substituents. Irradiation can be performed homogeneously, resulting in mixed ssDNA/OEG-AT monolayers of controlled composition (a), or by EBL, resulting in patterned ssDNA/OEG-AT features imbedded in a biologically inert matrix (c); b) chemical formulas of the monolayer components; c) AFM image of a representative A25SH/EG3 pattern prepared by IPER-EBL (5 s; 18×30 μm^2).

ing a respective increase of the A25SH component in the film (see Supporting Information, Figure S2). Significantly, no exchange occurs without irradiation as seen by the lack of the characteristic adenine signal for the control, non-irradiated sample (0 mC cm^{-2}) in Figure 2a. The thiolate anchoring of A25SH to gold in the mixed monolayers was proven by another control experiment where an irradiated EG3 film was exposed to non-thiolated homo-oligonucleotide (A25) as the substituent in IPER. No adenine signal was detected from this sample (second spectrum from the top in Figure 2a). Also, in agreement with the literature,[30] A25 is capable of binding directly on the gold surface (top spectrum in Figure 2a), but this does not occur when the gold is passivated and obscured by the EG3 film (even after the irradiation) because of the large steric requirement of binding A25 to gold, as compared to a gold-thiolate bond.[30] However, even in the case of thiolated ssDNA, its cross-section (approximately 154 Å^2; see Supporting Information) is significantly larger than that of the OEG-AT species (approximately 21.4 Å^2), which suggests

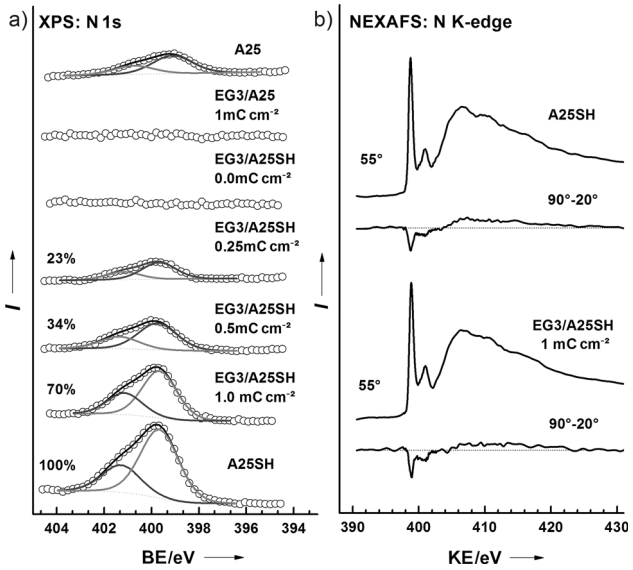

Figure 2. a) from bottom to top: N 1s PE spectra of the reference A25SH monolayer, mixed EG3/A25SH films prepared by IPER at different doses, non-irradiated (0 mC cm^{-2}) EG3 monolayer exposed to A25SH, irradiated (1 mC cm^{-2}) EG3 monolayer exposed to A25, and Au substrate exposed to A25. The proportions of A25SH in the reference and mixed films are given as percentages on each curve. b) N K-edge NEXAFS spectra (55°) of the reference A25SH monolayer and mixed EG3/A25SH film prepared by IPER (1 mC cm^{-2}) along with the difference between the spectra acquired at 90° and 20° of X-ray incidence. BE = binding energy; KE = kinetic energy.

that every exchange event within the IPER framework involves several constituents of the primary OEG-AT matrix. The most probable scenario is that the damaged OEG-AT species, which are only few in the given dose range, serve as initiator sites for the exchange reaction, which is thermodynamically driven and is initially mediated by the alkanethiol tail (note that there is no IPER without this part; see the results for A25) and later involves partial squeezing or expelling of several OEG-AT species adjacent to the defect site.

Further evidence for the formation of high-quality A25SH/EG3 monolayers was provided by near-edge X-ray absorption fine structure (NEXAFS) spectroscopy. As shown in Figure 2b, N K-edge spectra of the mixed films exhibit characteristic π* resonances of adenine at approximately 399.4 and 401.3 eV,[5,31] mimicking the spectrum of the one-component A25SH monolayer. The C K-edge NEXAFS spectra of the mixed films can be reproduced as linear combinations of the spectra of the both constituents, namely EG3 and A25SH (Supporting Information, Figure S3), which showed that their electronic structures are not affected by the mixing. Furthermore, the N K-edge NEXAFS spectra of the mixed films exhibit noticeable linear dichroism, similar to the spectra of the one-component A25SH monolayer, as manifested by the differences between the spectra acquired at the normal (90°) and grazing (20°) incidence angles of X-rays in Figure 2b. The negative peaks at the positions of the π* resonances of adenine indicate a parallel-to-the-substrate orientation of the nucleobases,[5,32] corresponding to an upright orientation of the DNA strands both in the one-component A25SH monolayer as well as in the mixed A25/EG3 films prepared by IPER.

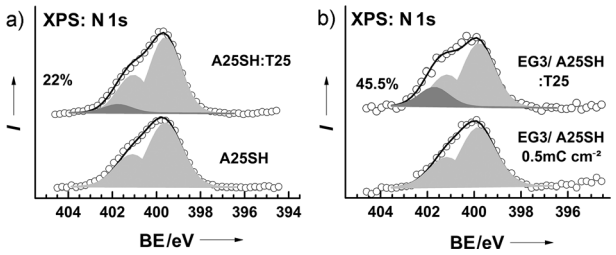

Figure 3. N 1s PE spectra of the reference A25SH monolayer (bottom, a) and mixed EG3/A25SH film fabricated by IPER with a dose of 0.5 mC cm^{-2} (bottom, b) along with the spectra of the same films after the hybridization with T25 (top, a,b). The spectra are decomposed into individual contributions, which are shaded light gray for adenine and dark gray for thymine. The decomposition procedure was performed self-consistently and relied on well-known data for adenine- and thymine-based oligonucleotides.[5,30] Note that the spectra in the bottom traces were used as references for the decomposition of the spectra in the top traces.

The mixed A25SH/EG3 films generated by IPER were tested for hybridization by exposing them to their complementary $d(T)_{25}$ strand, abbreviated T25. This exposure resulted in the appearance of the characteristic emission of thymine (T) at approximately 401.0 eV[5,30] in the N 1s PE spectra as shown in Figure 3b. The degree of hybridization was estimated at approximately 45.5% for the A25SH/EG3 monolayers prepared by IPER with a dose of 0.5 mC cm^{-2}. The efficiency of hybridization for this monolayer is much higher than that of the one-component A25SH film (approximately 22%; Figure 3a). This behavior can be attributed to the lower packing density of the ssDNA strands in the mixed films, which improves the steric access and diminishes electrostatic repulsion.

The above results demonstrate that mixed A25SH/EG3 monolayers of desirable composition can be fabricated by IPER, as long as the irradiation is performed homogeneously and the dose is controlled. We then adapted IPER in combination with EBL to fabricate complex nanopatterns of A25SH embedded in a protein-resistant EG3 matrix (Figure 1c). Using these patterns as templates, we grew them in the z-direction, making 3D DNA nanostructures, by using the 3′-ends of the surface-bound ssDNA (A25SH in this case) as initiation sites for SIEP of DNA by terminal deoxynucleotidyl transferase (TdT).[7,33] This step exploits the ability of TdT to sequentially add mononucleotides (adenine in this case) to the 3′-end of a ssDNA,[34] that is the polymerization of DNA with the chain length that can be adjusted from a few bases to several thousand bases.[35] We found that the density of ssDNA controls the feature height that is observed in the z-direction; for patterned regions with a high density of initiator strands, the growing chains formed a DNA brush with significant height, while a low density of initiator resulted in chains that are not confined, forming a structure with lower height.[25] For constant reactant concentration and time during SIEP, the height of the DNA brush should be proportional to the amount of A25SH in the mixed A25SH/EG3 films, as is indeed the case (Supporting Information, Figure S4). The identity and purity of the poly(A) brush is shown by a characteristic P 2p emission of ssDNA at 134.1 eV[36] and π* resonances of adenine in the N K-edge NEXAFS spectra (Supporting Information, Figure S5, S6), and other spectroscopic data, which will be published elsewhere. Furthermore, as seen in the above figures, no DNA brush or contamination-related features were observed for the one-component EG3 template, where without irradiation, no exchange with A25SH occurs. This guarantees, in agreement with previous studies,[28,29] a DNA-free protein-repelling background for growing ssDNA nanostructures on ssDNA/AT-OEG templates prepared by IPER-EBL.

We were able to fabricate DNA nanostructures of arbitrary shape in an EG3 matrix by EBL-IPER followed by SIEP, as shown in Figure 4 and Figures S7–S10, where several representative examples of poly(A) nanostructures are presented. Importantly, the ability to introduce gradients in the surface concentration of the A25SH by IPER allows the formation of nanostructures with a structural complexity that is not possible by other nanofabrication methodologies. The letters "DNA", wedges, and cone-like columns in Figure 4a–c were fabricated as gradient-like brushes; the respective height profiles (Figure 4a) agree well with the ellipsometric height of the homogeneous brush in Figure S4. The "amphitheater" structure in Figure 4d is an example of a more complex nanostructure. The maximum height of the brush patterns was approximately 150 nm (Figure 4c), which can be precisely controlled by two orthogonal experimental parameters: 1) the density of the A25SH moieties (which is controlled by the irradiation dose in IPER), and whose 3′ ends serve as initiation sites for SIEP, and 2) the experimental conditions of

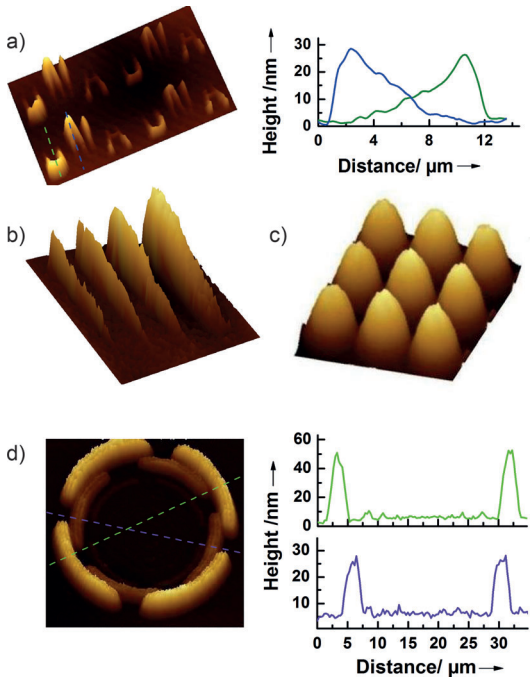

Figure 4. AFM images (3D view) of representative poly(A) brush patterns grown using SIEP on the EG3/A25SH templates prepared by IPER-EBL and the height profiles (a,d) along the lines of the respective color shown in the images. a) contrary-running gradient-like "DNA" letters, image 36×63 μm^2; b) wedges with widths of 2, 1, 0.5, and 0.25 μm, image 20×30 μm^2; c) cone columns, image 27×30 μm^2; d) a microscale "amphitheater", image 34×35 μm^2. Patterns were made in 22, 5, 54, and 14 s, respectively.

SIEP, namely the nucleotide concentration, enzyme-to-nucleotide ratio, and reaction time, which affect the chain length of each DNA strand. This process is somewhat analogous to photographic development in that the "negative" written by EBL in the EG3 matrix is "developed" by exchange with A25SH, and the fabricated A25SH pattern is then "amplified" by SIEP, becoming poly(A) 3D nanostructures embedded in the EG3 "background". Note that brush structures exhibit a slight expansion as compared to the template pattern, which becomes essential for nanometer scale features, putting certain limitations on the lateral size and height of these structures.[7,37] As for the template patterns, features down to 30–50 nm can be easily fabricated (Supporting Information, Figure S11).

In summary, we present a universal two-step procedure to fabricate mixed ssDNA/OEG-AT monolayers and patterns on gold substrates. The procedure is based on IPER and relies on commercially available compounds—making it easily accessible—and is highly flexible in terms of the composition of the mixed monolayers, as well as the size and shape of the DNA patterns that can be formed on the OEG-AT background. This approach is not limited to the compounds used herein but could be used with almost any combination of a protein-repelling OEG-AT SAM and thiolated ssDNA. The versatility of this approach is demonstrated by its combination with TdT-catalyzed SIEP that allows amplification of ssDNA/OEG-AT patterns in the *z*-direction. This combination provides a new method to sculpt complex 3D DNA nanostructures on solid supports.

Experimental Section

The EG3 and A25SH monolayers were prepared by immersion procedures, following standard methods. They were either homogeneously irradiated (10 eV; IPER) or patterned with a focused electron beam (1 keV, EBL-IPER) and exposed to A25SH for 3 h. The hybridization experiments were performed according to standard procedures.[4,5] The growth of poly(A) brushes was carried out according to modified methods,[7,30] as elaborated in the Supporting Information. The monolayers, homogeneous poly(A) brushes, and poly(A) nanostructures were characterized by both laboratory- and synchrotron-based PE spectroscopy, NEXAFS spectroscopy, ellipsometry, atomic force microscopy (AFM), and optical microscopy. For details and further references, see the Supporting Information.

Received: May 31, 2012
Revised: July 23, 2012
Published online: September 17, 2012

Keywords: chemical lithography · DNA structures · monolayers · nanostructures · polymer brushes

[1] J. J. Storhoff, C. A. Mirkin, *Chem. Rev.* **1999**, *99*, 1849 – 1862.
[2] N. C. Seeman, *Annu. Rev. Biochem.* **2010**, *79*, 65 – 87.
[3] V. Singh, M. Zharnikov, A. Gulino, T. Gupta, *J. Mater. Chem.* **2011**, *21*, 10602 – 10618.
[4] S. M. Schreiner, A. L. Hatch, D. F. Shudy, D. R. Howard, C. Howell, J. Zhao, P. Koelsch, M. Zharnikov, D. Y. Petrovykh, A. Opdahl, *Anal. Chem.* **2011**, *83*, 4288 – 4295.
[5] C. Howell, Y. Jeyachandran, P. Koelsch, M. Zharnikov, *J. Phys. Chem. C* **2012**, *116*, 11133 – 11140.
[6] M. Ritzefeld, N. Sewald, *J. Amino Acids* **2012**, DOI: 10.1155/2012/816032.
[7] D. C. Chow, W.-K. Lee, S. Zauscher, A. Chilkoti, *J. Am. Chem. Soc.* **2005**, *127*, 14122 – 14123.
[8] W. Y. Chen, W. P. Hu, Y. D. Su, A. Taylor, S. Jiang, G. L. Chang, *Sens. Actuators B* **2007**, *125*, 607 – 614.
[9] J. Ladd, A. D. Taylor, M. Piliarik, J. Homola, S. Jiang, *Anal. Chem.* **2008**, *80*, 4231 – 4236.
[10] T. M. Herne, M. J. Tarlov, *J. Am. Chem. Soc.* **1997**, *119*, 8916 – 8920.
[11] C. Boozer, S. Chen, S. Jiang, *Langmuir* **2006**, *22*, 4694 – 4698.
[12] P. Gong, C.-Y. Lee, L. J. Gamble, D. G. Castner, D. W. Grainger, *Anal. Chem.* **2006**, *78*, 3326 – 3334.
[13] A. Kick, M. Bönsch, K. Kummer, D. V. Vyalikh, S. L. Molodtsov, M. Mertig, *J. Electron Spectrosc. Relat. Phenom.* **2009**, *172*, 36 – 41.
[14] A. B. Steel, R. L. Levicky, T. M. Herne, M. J. Tarlov, *Biophys. J.* **2000**, *79*, 975 – 981.
[15] S. H. Brewer, S. J. Anthireya, S. E. Lappi, D. L. Drapcho, S. Franzen, *Langmuir* **2002**, *18*, 4460 – 4464.
[16] C. Y. Lee, P. Gong, G. M. Harbers, D. W. Grainger, D. G. Castner, L. J. Gamble, *Anal. Chem.* **2006**, *78*, 3316 – 3325.
[17] C. Bamdad, *Biophys. J.* **1998**, *75*, 1997 – 2003.
[18] C. Boozer, J. Ladd, S. Chen, Q. Yu, J. Homola, S. Jiang, *Anal. Chem.* **2004**, *76*, 6967 – 6972.
[19] X. Zhang, V. K. Yadavalli, *Biosens. Bioelectron.* **2011**, *26*, 3142 – 3147.
[20] Y. Nagasaki, *Polym. J.* **2011**, *43*, 949 – 958.
[21] W. P. Hu, L. Y. Huang, T. C. Kuo, W. W. Hu, Y. Chang, C.-S. Chen, H. C. Chen, W.-Y. Chen, *Anal. Biochem.* **2012**, *423*, 26 – 35.
[22] N. K. Devaraj, G. P. Miller, W. Ebina, B. Kakaradov, J. P. Collman, E. T. Kool, C. E. D. Chidsey, *J. Am. Chem. Soc.* **2005**, *127*, 8600 – 8601.
[23] C. Y. Lee, P. C. Nguyen, D. W. Grainger, L. J. Gamble, D. G. Castner, *Anal. Chem.* **2007**, *79*, 4390 – 4400; Gamble, D. G. Castner, *Anal. Chem.* **2007**, *79*, 4390 – 4400.
[24] N. Ballav, A. Shaporenko, A. Terfort, M. Zharnikov, *Adv. Mater.* **2007**, *19*, 998 – 1000.
[25] N. Ballav, S. Schilp, M. Zharnikov, *Angew. Chem.* **2008**, *120*, 1443 – 1446; *Angew. Chem. Int. Ed.* **2008**, *47*, 1421 – 1424.
[26] N. Ballav, A. Terfort, M. Zharnikov, *Langmuir* **2009**, *25*, 9189 – 9196.
[27] Y. L. Jeyachandran, M. Zharnikov, *J. Phys. Chem. C* **2012**, *116*, 14950 – 14959.
[28] S. Schilp, A. Rosenhahn, M. E. Pettitt, J. Bowen, M. E. Callow, J. A. Callow, M. Grunze, *Langmuir* **2009**, *25*, 10077 – 10082.
[29] N. Ballav, H. Thomas, T. Winkler, A. Terfort, M. Zharnikov, *Angew. Chem.* **2009**, *121*, 5947 – 5950; *Angew. Chem. Int. Ed.* **2009**, *48*, 5833 – 5836.
[30] A. Opdahl, D. Y. Petrovykh, H. Kimura-Suda, M. J. Tarlov, L. J. Whitman, *Proc. Natl. Acad. Sci. USA* **2007**, *104*, 9 – 14.
[31] Y. Zubavichus, A. Shaporenko, V. Korolkov, M. Grunze, M. Zharnikov, *J. Phys. Chem. B* **2008**, *112*, 13711 – 13716.
[32] J. Stöhr, *NEXAFS Spectroscopy*, Springer Series in Surface Science 25, Springer, Berlin, **1992**.
[33] D. C. Chow, A. Chilkoti, *Langmuir* **2007**, *23*, 11712 – 11717.
[34] K. Kato, J. M. Goncalves, G. E. Houts, F. J. Bollum, *J. Biol. Chem.* **1967**, *242*, 2780 – 2789.
[35] V. Tjong, H. Yu, A. Hucknall, S. Rangarajan, A. Chilkoti, *Anal. Chem.* **2011**, *83*, 5153 – 5159.
[36] N. Ballav, P. Kölsch, M. Zharnikov, *J. Phys. Chem. C* **2009**, *113*, 18312 – 18320.
[37] M. Steenackers, A. Küller, N. Ballav, M. Zharnikov, M. Grunze, R. Jordan, *Small* **2007**, *3*, 1764 – 1773.

